Article

Docking a bespoke ultra-large tetrahydropyridine library identifies 5-HT2A receptor agonists conferring new biology

https://doi.org/10.1038/s41586-019-0000-0

Received: 00 Month 20XX

Accepted: 00 Month 20XX

Published online: 00 Month 20XX

Anat Levit Kaplan†[1], Danielle N. Confair†[2], Kuglae Kim†[3,13], Ximena Barros-Álvarez†[4], Ramona M. Rodriguiz[5,6], Ying Yang[1], Oh Sang Kweon[2], Tao Che[7], John McCorvy[8], David N. Kamber[2], James P. Phelan[2], Luan Carvalho Martins[1,9], Vladimir M. Pogorelov[5], Jeffrey F. DiBerto[3], Samuel T. Slocum[3], Xi-Ping Huang[10], Jain Manish Kumar[3], Michael J. Robertson[4], Ouliana Panova[4], Alpay B. Seven[4], Autumn Q. Wetsel[5], William C. Wetsel[*5,6,11], John J. Irwin[*1], Georgios Skiniotis[*4], Brian K. Shoichet[*1], Bryan L. Roth[*3,12], Jonathan A. Ellman[*2].

Abstract There is much interest in screening ultra-large chemical libraries, both empirically and computationally. Both efforts have focused on readily synthesizable molecules, inevitably leaving many interesting chemotypes unexplored. Here we investigate structure-based docking of a bespoke virtual library of tetrahydropyridines (THPs), a scaffold poorly sampled by a general 1.35 billion-molecule make-on-demand virtual library but well-suited to many aminergic G protein-coupled receptors (GPCRs). Using three inputs, each with many diverse commercially available derivatives, a one pot C–H alkenylation, electrocyclization, and reduction sequence provides the tetrahydropyridine core with up to six sites of side chain derivatization. Restricting ourselves to tetrahydropyridines with MW <350 led to a virtual library of 75 million molecules. Docking these against a model of the serotonin 5-HT2A receptor (5-HT2AR) prioritized hundreds-of-thousands of molecules, of which 17 were initially synthesized and tested. Four had low μM activities against either the 5-HT2A or 5-HT2B receptors; one had weak antagonist activity against human 5-HT2AR. We optimized these leads using a cycle of design, synthesis, and testing for binding and function. This revealed 5-HT2AR agonists (R)-69 and (R)-70 with EC50s of 41 and 110 nM and unusual signaling kinetics that differ from psychedelic 5-HT2AR agonists. Cryo-EM structural analysis validated the predicted mode of binding to the 5-HT2AR. The favorable physical properties of these new agonists conferred high brain permeability, enabling mouse behavioral assays. Intriguingly, neither had psychedelic drug-like nor reinforcing activities, again in contrast to classic psychedelics. Significantly, both compounds had potent anti-depressant drug-like actions in mouse genetic and stress models, that were equi-efficacious to classic anti-depressants like fluoxetine (Prozac) at as little as 1/40th the

1. Department of Pharmaceutical Chemistry, University of California, San Francisco, CA, USA, 2. Department of Chemistry, Yale University, New Haven, CT, USA , 3. Department of Pharmacology, University of North Carolina, Chapel Hill School of Medicine, Chapel Hill, NC, USA, 4. Department of Molecular and Cellular Physiology, Stanford University School of Medicine, Stanford, CA, USA, 5. Department of Psychiatry and Behavioral Sciences, Duke University Medical Center, Durham, NC, USA, 6. Mouse Behavioral and Neuroendocrine Analysis Core Facility, Duke University Medical Center, Durham, NC, USA, 7. Center for Clinical Pharmacology, Department of Anesthesiology, Washington University School of Medicine, Saint Louis, MO, USA, 8. Medical College of Wisconsin, Department of Cell Biology, Neurobiology and Anatomy, Milwaukee, WI, USA, 9. Biochemistry Department, Institute for Biological Sciences, Federal University of Minas Gerais, Belo Horizonte, Brazil, 10. National Institute of Mental Health Psychoactive Drug Screening Program, University of North Carolina Chapel Hill School of Medicine, Chapel Hill, NC, USA, 11. Departments of Cell Biology and Neurobiology, Duke University Medical Center, Durham, NC, USA, 12. Division of Chemical Biology and Medicinal Chemistry, Eshelman School of Pharmacy, University of North Carolina Chapel Hill, NC, USA, 13. Department of Pharmacy, Yonsei University, Incheon, Republic of Korea† These authors contributed equally., * Corresponding authors.

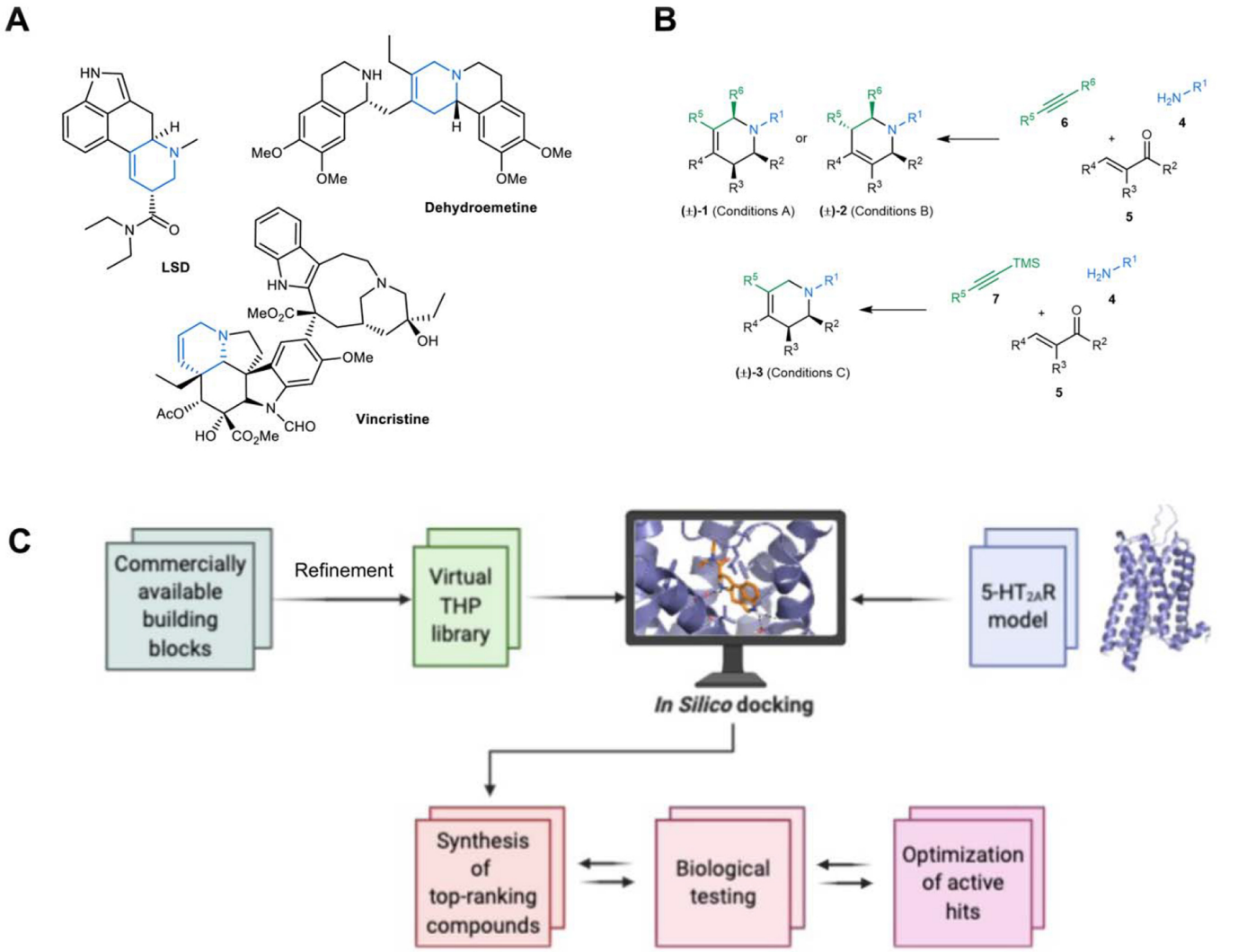

Figure 1. Bespoke ultra-large virtual library approach. (A) Drugs containing the tetrahydropyridine motif. (B) Three types of tetrahydropyridines ( )-1 to ( )-3 from commercially available alkynes 6 and 7, primary amines 4, and α,β-unsaturated carbonyl compounds 5. (C) Generation of a virtual library of 75 million tetrahydropyridines for docking against a homology model of the 5-HT2AR.

dose. Prospects for using bespoke virtual libraries to deepen sampling of pharmacologically-relevant chemical space will be considered.

Introduction

The advent of DNA-encoded and virtual libraries has led to a renaissance in ultra-large sets of molecules in early ligand discovery.1 In particular, the virtual libraries now exceed 20 billion enumerated, readily accessible molecules. In docking screens, these virtual libraries have explored new chemotypes well-suited to receptor sites, discovering ligands with potencies in the mid-pM to low-nM range2-4. This represents a substantial improvement from screens of smaller, "in-stock" libraries of several million molecules against the same targets. The virtual libraries enumerate diverse chemotypes, reflecting the synthetic products of >120,000 building-blocks synthesized via >140 two-component reactions. Nevertheless, the vastness of chemical space ensures that many interesting chemotypes are inevitably absent or under-sampled by both virtual and DNA-encoded libraries.

The six-membered nitrogen heterocycles piperidine and pyridine are two of the top three most frequent ring systems among FDA approved drugs (Table 1). In particular, the non-aromatic piperidine scaffold has several desirable features, such as a basic nitrogen that contributes to aqueous solubility and hydrogen-bonding interactions, high sp3 content with a three-dimensional rather than planar display5, and multiple sites for introducing substituents including at stereogenic centers. Tetrahydropyridines (THP) are a much less investigated class of six-membered nitrogen heterocycles that are intermediate in unsaturation between pyridines and piperidines with the same positive attributes as piperidines. While THPs are present in several natural product-derived drugs that include the psychedelic lysergic acid diethylamide (LSD), the antimigraine drug ergotamine, anticancer agents like vinblastine and vincristine, and the antiprotozoal agent dehydroemetine (Figure 1A)6, the scaffold is under-represented in most libraries compared to its congeners piperidine and pyridine (Table 1). In particular, while piperidine and pyridine compose a startling 16 to 18% of the unbiased REAL make-on-demand library, THPs make up only 0.35% of it (Table 1).

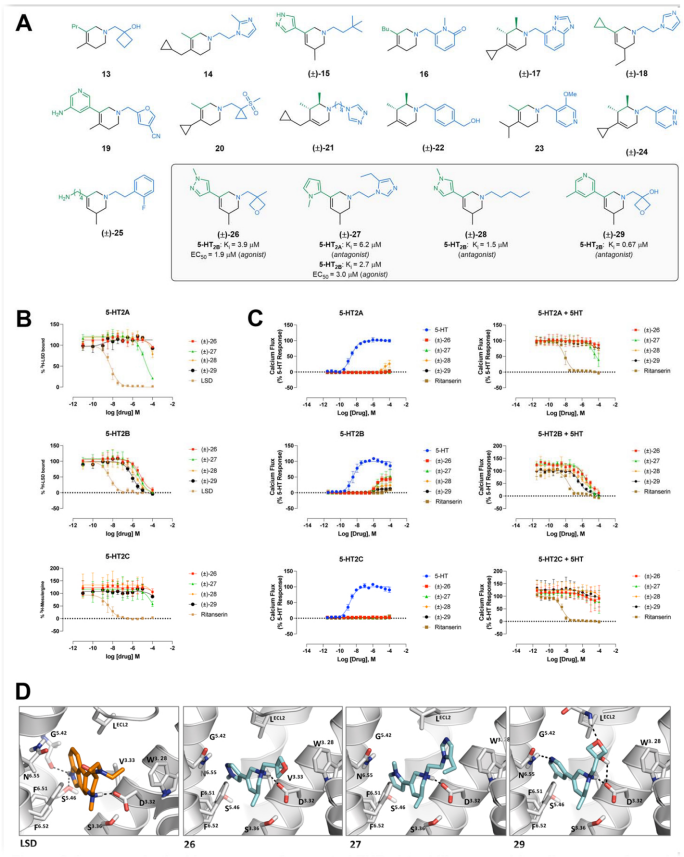

Figure 2. Large scale docking screen of a curated THP virtual library enables discovery of novel 5-HT2R ligands. (A) The initial 17 compounds synthesized and assayed; of these four had 5-HT2AR or 5-HT2BR activity (boxed). (B) Binding properties of the 4 hits at human 5-HT2Rs in radioligand competition binding assays. Concentration-inhibition curves for 4 hits at 5-HT2AR and 5-HT2BR versus [3H-LSD, and 5-HT2CR versus [3H]- Mesulergine. [3H]-LSD, and [3H]-Mesulgergine concentrations of 0.5 nM, and 1.0 nM were used, respectively. KD values of [3H]-LSD at human 5-HT2AR and 5-HT2BR were 0.33 and 0.91 nM, respectively, and KD value of [3H]-mesulergine at human 5-HT2CR was 0.67 nM21,28. LSD (5-HT2AR, 5-HT2BR) and Ritanserin (5-HT2CR) were used as positive controls. (C) Concentration-response curves of the 4 hits at stable 5-HT2AR, 5-HT2BR, and 5-HT2CR-INI Flp-In293 cell lines in Ca2+ assays. (D) Docked poses of characteristic docking actives compared to that of LSD (left panel). In all panels the Ballesteros-Weinstein numbering is shown in superscript for each residue.

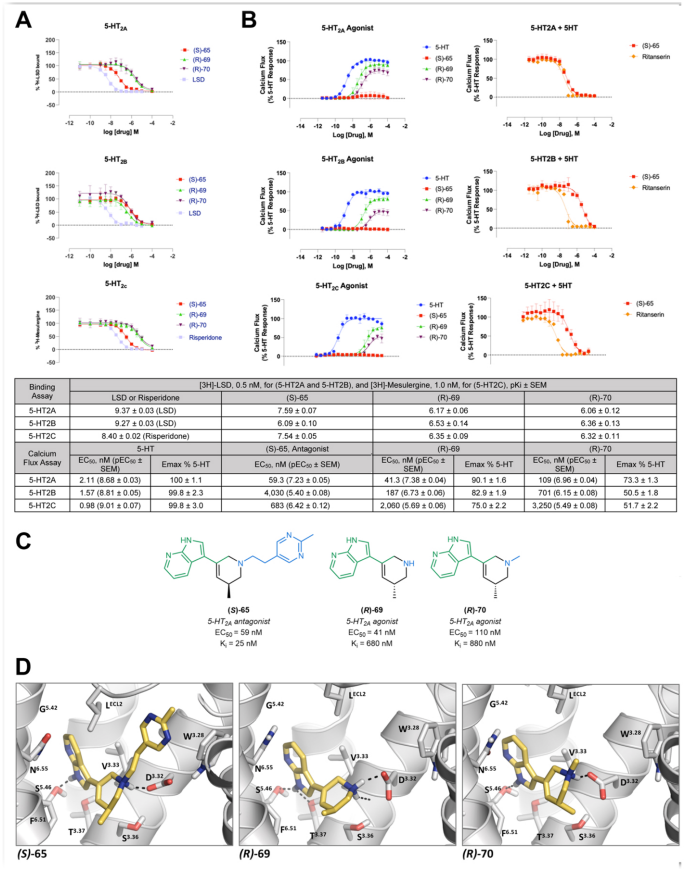

Binding Assay	[3H]-LSD, 0.5 nM, for (5-HT2A and 5-HT2B), and [3H]-Mesulergine, 1.0 nM, for (5-HT2C), pKi ± SEM			
	LSD or Risperidone	(S)-65	(R)-69	(R)-70
5-HT2A	9.37 ± 0.03 (LSD)	7.59 ± 0.07	6.17 ± 0.06	6.06 ± 0.12
5-HT2B	9.27 ± 0.03 (LSD)	6.09 ± 0.10	6.53 ± 0.14	6.36 ± 0.13
5-HT2C	8.40 ± 0.02 (Risperidone)	7.54 ± 0.05	6.35 ± 0.09	6.32 ± 0.11

Calcium Flux Assay	5-HT	(S)-65, Antagonist		(R)-69		(R)-70	
	EC50, nM (pEC50 ± SEM)	Emax % 5-HT	EC50, nM (pEC50 ± SEM)	EC50, nM (pEC50 ± SEM)	Emax % 5-HT	EC50, nM (pEC50 ± SEM)	Emax % 5-HT
5-HT2A	2.11 (8.68 ± 0.03)	100 ± 1.1	59.3 (7.23 ± 0.05)	41.3 (7.38 ± 0.04)	90.1 ± 1.6	109 (6.96 ± 0.04)	73.3 ± 1.3
5-HT2B	1.57 (8.81 ± 0.05)	99.8 ± 2.3	4,030 (5.40 ± 0.08)	187 (6.73 ± 0.06)	82.9 ± 1.9	701 (6.15 ± 0.08)	50.5 ± 1.8
5-HT2C	0.98 (9.01 ± 0.07)	99.8 ± 3.0	683 (6.42 ± 0.12)	2,060 (5.69 ± 0.06)	75.0 ± 2.2	3,250 (5.49 ± 0.08)	51.7 ± 2.2

Figure 3. Structure-guided discovery of novel 5-HT2AR agonists and antagonists. (A) Dose response competition binding assays of (S)-65, (R)-69, and (R)-70 against [3H]-LSD for 5-HT2AR and 5-HT2BR, and [3H]-Mesulergine for 5-HT2CR. [3H]-LSD and [3H]-Mesulgergine concentrations of 0.3 nM and 1 nM were used, respectively. LSD (5-HT2AR, 5-HT2BR) and Risperidone (5-HT2CR) were used as positive controls. (B) Concentration-response curves of (S)-65, (R)-69, and (R)-70 at stable 5-HT2AR, 5-HT2BR, and 5-HT2CR-INI Flp-In293 cell lines in Ca2+ assays. (R)-69 and (R)-70 show strong partial Gq agonist activities, whereas (S)-65 lacks agonist activity and instead shows antagonist activity. Data in (A) and (B) represent the mean ±S.E.M. from n=3 independent experiments. The pKi/EC50 values were compared using a one-way ANOVA with Dunnett's post-test (* = p<0.05, ** = p<0.01, *** = p<0.001, and **** = p<0.0001). (C) 2D structures, binding and functional affinities for the identified hits across the 5-HT2R subtypes. (D) Docking poses of the identified hits (S)-65 (left panel), (S)-69 (which scored better; middle panel) and (R)-70 (right panel). 5-HT2AR is shown in gray, the docked compounds are shown as capped sticks with carbons colored in yellow. In all panels the Ballesteros-Weinstein numbering is shown in superscript for each residue.

Obtaining a diverse display of functionality at different sites about the 6-membered ring in piperidines and THPs is synthetically challenging. Recently, we have described new, convergent routes to access three THP subtypes [( )-1 to ( )-3] with six sites of derivatization from commercially available starting materials (Figure 1B)7-9. The large space defined by such derivatives, along with their functionally congested, geometrically complex structures, and their under-representation in general libraries (Table 1)10, makes them interesting to explore as central scaffolds for large virtual libraries eminently suitable for structure-based molecular docking campaigns.

Accordingly, we calculated a library of over 75 million potential tetrahydropyridines, built around commercially available building blocks and restricted to products with "lead-like" physical properties (e.g., < 350 amu, cLogP < 3.5)11,12. The cationic nature of these molecules at physiological pH makes them suitable as ligands for aminergic GPCRs, including the 5-HT2A serotonin receptor (5-HT2AR). The 5-HT2AR is a target of much interest, owing to its role in psychiatric disorders including schizophrenia and related psychotic disorders, depression, and anxiety13-15. The 5-HT2AR also represents the canonical molecular target for LSD-like psychedelic drugs16, which have recently gained prominence as potential therapeutics for depression and anxiety17. A goal for therapeutics in this area is the development of molecules that retain anti-depressant and anxiolytic properties without hallucinogenic activity. Progress towards therapeutic leads and chemical probes against the 5-HT2AR has been slowed by the need for selectivity over related off-targets, such as 5-HT2BR, versus other receptors such as the serotonin transporter (SERT), and for functional selectivity in signaling (i.e., for G protein vs. -arrestin recruitment16,18-21). Collectively, these features make the 5-HT2AR a therapeutically worthy yet challenging target. Meanwhile, the receptor's small and well-formed

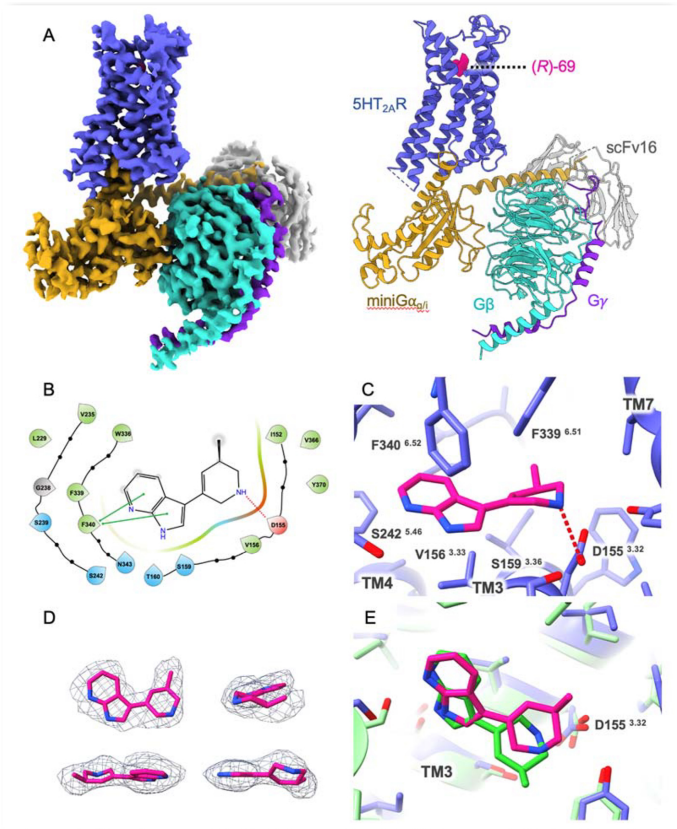

Figure 4. Structure of 5-HT2AR bound to (R)-69 by cryo-EM. (A) Overall cryo-EM map (left) and model (right) of 5-HT2AR bound to the novel strong partial agonist (R)-69 in complex with mini-Gq/i. (B) Schematic of ligand-specific interactions of (R)-69 with 5-HT2AR orthosteric binding site residues. A salt bridge with D1553.32 is shown as a red dashed line. Color code for residues and interactions: green: hydrophobic, blue: polar, red: negatively charged, grey: glycine, green solid line: Pi-Pi stacking interaction. (C) Specific residues in the binding pocket that interact with (R)-69 are shown as sticks and labeled. (R)-69 is shown as magenta-colored sticks. A salt bridge with D1553.32 is shown as a red dashed line. (D) Cryo-EM density for (R)-69. (E) Comparison of the computationally predicted and experimentally resolved binding poses of (S)-69 and (R)-69, respectively. The experimentally determined cryo-EM structure in magenta is superposed onto the pose of (S)-69 docked to the 5-HT2AR homology model in green. Ballesteros-Weinstein numbering is shown in superscript for each residue in panels (C) and (E).

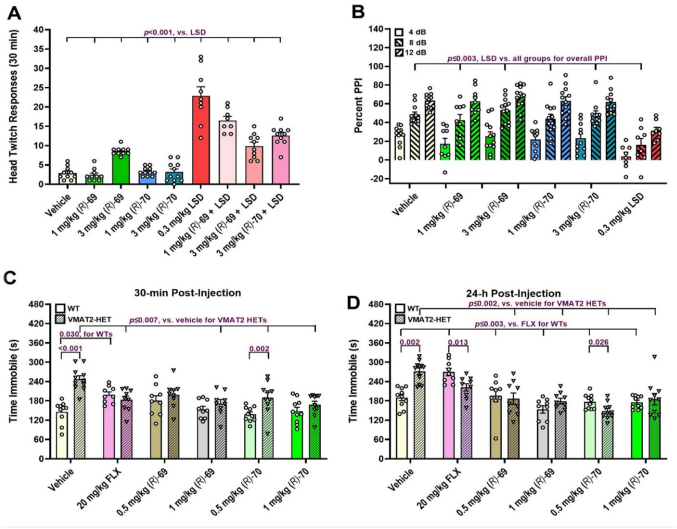

Figure 5. Head twitch, PPI responses, and anti-depressant-like actions of (R)-69 and (R)-70 in VMAT2 mice. (A) Head twitch responses (HTRs) in C57BL/6J mice during the first 30 min after injection (i.p.) of the vehicle, 1 or 3 mg/Kg (R)-69, 1 or 3 mg/Kg (R)-70, 0.3 mg/Kg LSD, 1 or 3 mg/Kg (R)-69 + 0.3 mg/Kg LSD, or 3 mg/Kg (R)-70 + 0.3 mg/Kg LSD. HTRs are low in the (R)-69 and (R)-70 groups and they partially block the LSD effects. (B) PPI in C57BL/6J mice treated (i.p.) with vehicle, 1 or 3 mg/Kg (R)-69, 1 or 3 mg/Kg (R)-70, or 0.3 mg/Kg LSD. PPI is unaffected with (R)-69 or (R)-70 relative to the vehicle and the LSD disruption. (C-D) Immobility in tail suspension at 30 min and 24 h with WT and VMAT2 heterozygous (HET) mice after a single injection (i.p.) of vehicle, 20 mg/Kg fluoxetine (FLX), 0.5 or 1 mg/Kg (R)-69, or 0.5 or 1 mg/Kg (R)-70. Acute genotype differences are seen with the vehicle and 0.5 mg/Kg (R)-70; at 24 h effects are present with the vehicle, fluoxetine, and 0.5 mg/Kg (R)-70. In WT mice immobility to acute administration of FLX is enhanced relative to vehicle and at 24 h it is increased with FLX compared to the vehicle, and 0.5 and 1 mg/Kg (R)-69 and (R)-70. In VMAT2 HETs, 30-min after administration FLX, 1 mg/Kg (R)-69, and 0.5 and 1 mg/Kg (R)-70 reduce immobility and at 24-h 0.5 and 1 mg/Kg (R)-69 and (R)-70 are also efficacious compared to the vehicle control. Statistics in Ext. Data Table 5, Bonferroni p-values (ps) across multiple comparisons showing the lowest value closest to p<0.05

orthosteric site16 makes it a favorable target for docking this particular virtual library.

We therefore explored docking to prioritize selective 5-HT2AR ligands from among the 75 million molecule virtual library. Here we consider the mechanics of calculating a large library around a specific scaffold and reaction, of synthesizing docking-prioritized molecules from such a large space, and whether this approach to discover and optimize potent and selective ligands is useful. Implications for the creation and exploration of bespoke libraries around interesting scaffolds more generally will also be considered.

Results

Virtual library calculation. Tetrahydropyridine subtypes ( )-1 and ( )-2 were prepared from three readily available inputs: primary amines 4, α,β-unsaturated carbonyl compounds 5, and internal alkynes 6 (Figure 1B). Tetrahydropyridine subtype ( )-3 was prepared from primary amines 4, α,β-unsaturated carbonyl compounds 5, and trimethylsilyl (TMS) alkynes 7. A broad range of functional groups, including many different types of nitrogen heterocycles, were found to be compatible with the reaction sequence as determined by a functional group screen (Supplementary Figure 1). Heterocycle N–H functionality was incompatible with the chemistry, but this could be overcome by straightforward N-protection. Consequently, these inputs and restraints were also included in the virtual library. To simplify library synthesis and analysis, only achiral, single isomer inputs were included. Inputs with undesirable functionality like nitro groups, or molecules with too many rotatable bonds, were discarded. To generate library members with druglike physical properties, a molecular weight cutoff of 140 amu was applied to each of the reactants (TMS alkynes 7 were assigned a cutoff of 212 amu because the TMS group is cleaved during the synthesis). A molecular weight cutoff of 400 amu and a cLogP of < 3.5 were then applied to the assembled THPs ( )-1 to ( )-3 to furnish a virtual library of 4.3 billion compounds; this library would subsequently be available for selection of analogs. To maximize the likelihood of identifying hits with high ligand efficiency for the initial docking screen, we further restricted the molecular weight to < 350 amu, resulting in an initial virtual library of 75 million molecules.

Docking & modeling. Seeking novel ligands for the 5-HT2AR, we used an iterative computational and empirical screening strategy (Figure 1C). We initially did not differentiate between agonists or antagonists,

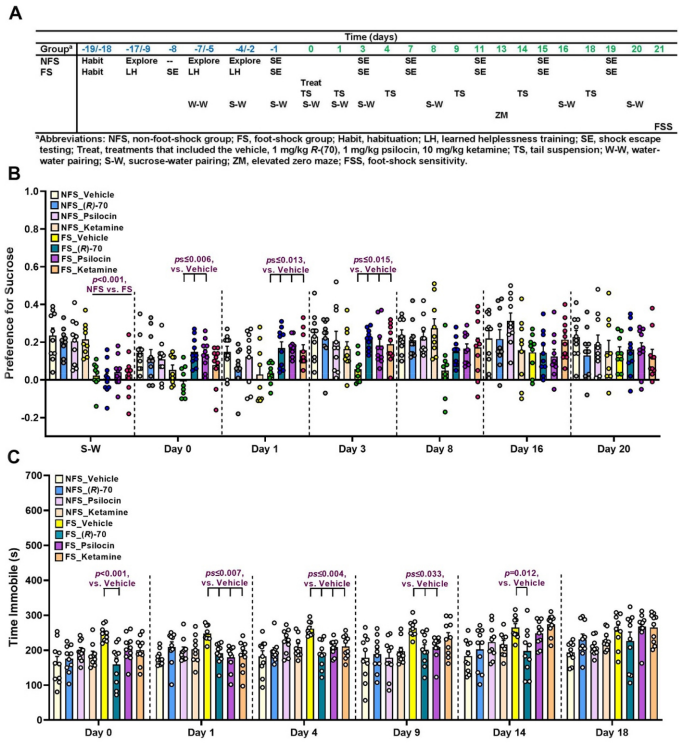

Figure 6. Experimental design, sucrose preference, and tail suspension for the learned helplessness experiment. (A) Experimental design. (B) Sucrose preference in C57BL/6 mice assigned to the non-foot-shock (NFS) and foot-shock (FS) conditions and treated (i.p.) with vehicle, 1 mg/Kg (R)-70, 1 mg/Kg psilocin, or 10 mg/Kg ketamine. During the initial sucrose-water (S-W) pairing, mice in the FS condition have a lower preference for sucrose than the NFS mice. Among the NFS mice, no treatment effects are found within days. By comparison among FS mice, sucrose preference is reduced in the vehicle-treated mice compared to the (R)-70 and psilocin groups on days 0, 1, and 3. The effects of ketamine are delayed and they become manifest on days 1 and 3. (C) Tail suspension testing in the same mice. Times of immobility are low and stable across time in the NFS mice. In the FS condition, 30-min following treatment (day 0), immobility is high in the vehicle control relative to the (R)-70 group and this effect persists through day 14. Relative to the FS vehicle control, psilocin and ketamine show efficacy on days 1 and 4, with the effects of psilocin lasting through day 9 post-injection. Statistics in Ext. Data Table 5, Bonferroni p-values (ps) across multiple comparisons showing the lowest value closest to p<0.05 or within a single comparison (p) from the vehicle (panels B-C) or condition (panel B).

since selective compounds of either class would be useful. As there were no X-ray or cryo-EM structures of the 5-HT2AR available at the time this study was conducted, we first built 1000 homology models templated on the 5-HT2BR X-ray structure bound to LSD, using Modeller (PDB ID: 5TVN, as described in ref. 21). The orthosteric ligand LSD was retained during the modeling to ensure a ligand-competent orthosteric binding site. The resulting homology models were evaluated for their ability to enrich 34 known 5-HT2AR ligands from the IUPHAR database22 versus 1899 property matched decoys23. The models were ranked by their ability to enrich the ligands vs. the decoys, in sensible geometries, among the top scoring docked molecules24,25. Models were also assessed for their ability to reproduce the crystallographic pose of LSD and to form key interactions with the receptor such as the observed salt bridge with Asp3.32.

The best performing 5-HT2AR model was screened against the 75 million THP library. Each library molecule had an average of 92 conformations calculated for it and was sampled in approximately 23,000 orientations. A total of 7.46 trillion complexes were sampled and scored; the calculation took 8,698 core hours, or just under 9 hours on 1000 cores of our lab cluster. The 300,000 top-ranking docked molecules were clustered by topological similarity, using an ECFP4-based Tanimoto coefficient (Tc) > 0.5, resulting in 14,959 non-redundant clusters. The cluster heads for the top ranked 4,000 clusters were then inspected for unfavorable features, which are sometimes not accounted for by the docking scoring function, including internal ligand strain and the occurrence of unsatisfied ligand hydrogen-bond donors, and for modeled interactions with key binding site residues26. Of those that remained, 205 were filtered for chemical novelty by insisting on ECFP4-based Tc values < 0.35 vs. ~28,000 annotated dopaminergic, serotoninergic, and adrenergic ligands from the ChEMBL20 database27.

Initial synthesis and testing. From the remaining top-ranking clusters, we synthesized 17 richly functionalized THPs. The selected primary amines 4 and α,β-unsaturated carbonyls 5 were first condensed to provide α,β-unsaturated imines 8 (Extended Data Fig. 1A). A one-pot reaction sequence then furnished THP sub-types ( )-1 to ( )-3 by Rh(I)-catalyzed C–H addition of imine 8 to alkyne inputs 6 or 7 with in situ electrocyclization to give dihydropyridines (DHPs) ( )-9 or ( )-10, respectively. THPs ( )-1 to ( )-3 were obtained by submitting DHPs ( )-9 or ( )-10 to different reduction protocols without any work-up or isolation. To facilitate the synthesis of some initial compounds, and for later analog synthesis (vide infra), a route was developed for the late-stage introduction of various R1 substituents on the nitrogen of the THP core by preparing THPs ( )-2 to ( )-3 with a cleavable substituent on the nitrogen (Extended Data Fig. 1B). The synthesized THPs display a range of interesting functionalities and are well-differentiated from the endogenous agonist, serotonin, and from previously reported 5-HT2AR synthetic ligands.

The initial set of 17 synthesized THPs were tested in radioligand displacement assays versus the 5-HT2AR, 5-HT2BR and 5-HT2CR subtypes. This identified four molecules with Ki values ranging from 0.67 to 3.9μM, a 24% hit rate (Figure 2A-B). In functional assays at the three 5-HT2R subtypes, these four ligands exhibited either agonist or antagonist activity, with agonist activity ranging from 1.9 to 3.0 μM at the 5-HT2BR (Figure 2C, Extended Data Table 1).

Docked poses of the confirmed ligands suggested that all four interact with conserved binding site residues, including a salt bridge between the THPs' tertiary amine and D1553.32, a characteristic interaction in aminergic and certainly serotonergic29 GPCRs (Figure 2D). Several of the THPs were also predicted to hydrogen bond with N3436.55 on TM6 and the main chain of residues on the second extracellular loop (ECL2), and to form van der Waals interactions with residues on transmembrane helices 3, 5 and 6. Since the 5-HT2AR and 5-HT2BR orthosteric binding sites are highly conserved, with only four residues varying between them16, we hypothesized that even THP ligands binding primarily at the 5-HT2BR subtype could be optimized to engage the 5-HT2AR.

Structure-based optimization. We initially focused on synthesizing THP analogs that conserved the pyridine and pyrazole substituents at the C5 position, while varying the substituent on the THP nitrogen. This substitution site showed greater variability in the early ligands and is also straightforward to modify from the many available building blocks. Twenty analogs incorporating the pyridine ring at the C5 position were synthesized and assayed for binding, initially as racemates. Several had improved affinity, and even those analogs with reduced affinity provided useful insights into structure activity relationships. Although the 3-hydroxyoxetane functionality was developed as a carboxylic acid bioisostere30, the corresponding carboxylic acid analog ( )-30 had no activity against the 5-HT2AR or 5-HT2BR (Supplementary Figure 2A). However, the oxygen heteroatoms in the hydroxyoxetane do contribute to binding because the 1-methylcyclobutyl ( )-31 and neopentyl ( )-32 analogs had reduced affinity. The location of the basic pyridyl nitrogen is also important as established by the lack of activity of the pyridine regiosomer ( )-33.

The eight highest affinity racemic analogs were separated by chiral high-performance liquid chromatography (HPLC) and tested for binding and functional activity as single enantiomers (Extended Data Table 2). As exemplified for (R)-35 and (S)-35, strong chiral discrimination was generally observed for the binding of each pair of enantiomers to both 5-HT2AR and 5-HT2BR. Encouragingly, docking correctly predicted that the S-enantiomer would bind with greater affinity. Improved binding affinity and functional activity was observed when the methyl substituent present on the pyridyl ring was replaced by the isosteric but metabolically stable chloro substituent, as exemplified by (R)/(S)-35 and (R)/(S)-36. Based upon the incipient 5-HT2BR hit ( )-28 (Extended Data Table 1), the pentyl substituent was introduced on the THP nitrogen of (S)-37, resulting in sub-micromolar agonist activity at the 5-HT2AR, though still with ~10-fold greater agonism of the 5-HT2BR. Analogs with variable alkyl chain lengths and branching were low nanomolar agonists of the 5-HT2BR, but unfortunately did not improve agonist activity at the 5-HT2AR.

The C5-pyrazole substituent is present in two of our four initial active ligands. To capitalize on this substituent, we revisited the 4.3 billion compound virtual library with molecular weights < 400 amu. Library members with a Tanimoto similarity of > 0.5 to initial hits ( )-26 and ( )-28 were docked to the 5-HT2AR orthosteric binding site and their poses assessed for steric complementarity and for favorable interactions with binding site residues. While numerous substituents with diverse steric profiles and hydrogen bonding abilities were examined off the THP nitrogen (( )-43-( )-54), in all cases binding affinity of > 10μM was observed at the 5-HT2AR (Supplementary Figure 2B). We also experimented with introducing nitrogen substituents from the other initial hit compounds in analogs ( )-55 and ( )-56 but found these changes to be unfavorable. The larger ethyl rather than a methyl substituent, at either C3 (( )-57) or on the pyrazole nitrogen (( )-58), was not tolerated.

Searching the greater 4.3 billion compound virtual library for similar compounds with heteroaryl groups to replace the pyrazole substituent proved to be more successful, with the azaindole substituent resulting in improved affinity and functional activity. Fourteen azaindole analogs were separated and tested as single enantiomers, with most exhibiting partial or full agonism at the 5-HT2AR (Extended Data Table 3). Small nitrogen substituents provided the greatest agonist activity and led to the identification of 5-HT2AR strong partial agonists (R)-69 and (R)-70 with 41 nM and 110 nM EC50 values in a calcium flux assay, respectively (Figure 3A-C). In contrast, introduction of the larger 2-(3-(2-methylpyrimidinyl))ethyl nitrogen substituent provided a selective 5-HT2AR antagonist (S)-65 with 59nM activity (Figure 3; Extended Data Table 3). The strong partial agonists (R)-69 and (R)-70 were structurally similar to the initial docking hits, including C5 placement of a heteroaromatic ring and the importance of both unsaturation and the C3 methyl substituent in the THP ring (see 71 and 72).

Target & functional selectivity. Selective activity on 5-HT2AR versus off-targets like the highly-related 5-HT2BR, other serotonin receptors—metabotropic but also ionotropic—and even transporters is important for usefulness as chemical probes and for therapeutic potential (for instance, 5-HT2BR agonists can cause valvular heart disease)18. (R)-69 had an agonist EC50 of 190 nM vs. 5-HT2BR, making it 4.6-fold selective for the 5-HT2AR, while (R)-70 is 6.4-fold selective for 5-HT2AR versus 5-HT2BR (Figure 3C); the two compounds were 29 to 51-fold selective versus 5-HT2cR. Against a panel of 318 other GPCRs in a -Arrestin recruitment assay31, neither (R)-69 nor (R)-70 had measurable agonism, nor did either antagonize the hERG ion channel, a toxicology anti-target, up to 10 M (Extended Data Fig. 2A-C). By ligand displacement, no substantial binding was measured at 45 other off-targets (Extended Data Table 4 and SI Table 3). While (R)-69 had modest (0.8 M) activity for the serotonin transporter, SERT, (R)-70 had no measurable activity, and neither compound was active versus the DAT or NET transporters. Compared to classic psychedelic 5-HT2AR agonists like LSD, psilocin and DMT32, the new agonists are selective against most common serotonergic off-targets (Extended Data Fig. 2D-F). While the EC50 of even (R)-69, at 41 nM, can seem modest, we note that it is within the range of many in vivo active 5HT2A receptors agonists, including mescaline (4 M) psilocin (24 nM), LSD (6.4 nM), and lisuride (17 nM), while its selectivity versus 5HT2b and especially 5HT2c is substantially higher than these classic and hallucinogenic agonists. Meanwhile, the optimized tetrahydropyridines have unusually high ligand efficiencies, reaching 0.6 kcal/HAC, contributing to the high brain exposure achieved by the molecules and to their in vivo efficacy (below).

Unlike psychedelic 5-HT2AR agonists like LSD, which are arrestin-biased16,20,21,33, the new agonists were G protein biased, activating Gq signaling at mid-nanomolar concentrations with high efficacy while Arr2 recruitment was only detectable at higher concentrations. To quantify these differential kinetics, we calculated transduction coefficients at each time point for Gq and Arr2 activities. (R)-69 and (R)-70 displayed stable differences unlike the other tested 5-HT2AR ligands, which had more variable patterns (Extended Data Fig. 3).

Structure prediction and determination by cryo-EM. Since the S-enantiomer docked better during hit optimization, we sought to refine the docked pose of (S)-69, as it would be important for further optimization of this series. Starting with the homology model of 5-HT2AR used in the ligand discovery phase, 40 ligand poses were generated. These were clustered into six poses and used as starting points for 50ns molecular dynamics (MD) simulations. Two stable poses emerged and were used to run retrospective free energy perturbation (FEP)34 for analogs of (S)-69, comparing these with experimentally measured binding affinities; the ligand-receptor complex whose relative affinities by FEP corresponded most closely to those of the analogs within this series was chosen as the final predicted pose (Supplementary Figure 3). The pose features a salt bridge with D1553.32, a hydrogen bond with S2425.46, and packing interactions with F2226.52 (superscripts refer to the Ballesteros–Weinstein numbering system for GPCR residues, where the first number denotes the helix and the second number indicates the residue position relative to the most conserved residue, defined as X.5035).

To template future compound optimization, understand activity at atomic resolution, and to test the predicted structures, we determine the structure of 5-HT2AR bound to (R)-69 by single particle cryogenic electron microscopy (cryoEM). We used our previously reported strategy16 in which the 5-HT2AR/miniGq complex was formed from separately purified receptor in the presence of (R)-69 and miniGq heterotrimer and further stabilized through the binding of a single-chain variable fragment (scFv16)36. We obtained the cryo-EM structure of the complex at a global nominal resolution of 3.4 Å (Figures 4A and Supplementary Figure 4; Supplementary Table 2).

The high quality cryo-EM density in the 5-HT2AR orthosteric site allowed for unambiguous modelling of (R)-69 (Figure 4D), which was further confirmed through the GemSpot pipeline37. Interactions with the orthosteric site residues include the key salt bridge interaction with D1553.32, and a -stacking interaction between the azaindole of (R)-69 and F3406.52 (Figure 4B and 4C). Multiple additional hydrophobic interactions including V1563.33, V2355.39, W3366.48 and F3396.51, also seem to play a role in (R)-69 binding. Although other polar interactions may be present in (R)-69 binding, no hydrogen-bond interaction is observed with the orthosteric site residues S2395.43, S2425.46 or S1593.36 involved in LSD and 25CN-NBOH (a N-benzyl phenethylamine full-agonist16) binding, respectively.

The superposition of the docked (S)-69 and experimental (R)-69 bound 5-HT2AR structures reveals good correspondence, with the azaindole groups superimposed almost identically (Figure 4E). The cryo-EM structure shows that the (R)-69 THP ring adopts a slightly different conformation to the computationally predicted one, with the C3 methyl substituent pointing to the extracellular side of the binding pocket. Nonetheless, the key interaction between the THP ring amine and the D1553.32 carboxylate is present as designed.

The cryo-EM structure of (R)-69 bound 5-HT2AR/miniGq/i informs comparisons with other 5-HT2AR structures (Extended Data Fig. 4). As with our previously described structure of 25CN-NBOH-bound 5-HT2AR in complex with a G protein (PDB: 6WHA16), reflecting the activated state of the receptor, the intracellular ends of TM5 and TM6 in the (R)-69 bound 5-HT2AR/miniGq/i adopt an open conformation accommodating the binding of the G protein -5 helix (Extended Data Fig. 4A). 5-HT2AR - miniGq/i interactions are virtually identical to those described for 25CN-NBOH, supporting the significance of 5-HT2AR residues N1072.37, D1723.49, N3176.29, and N3848.47 in hydrogen-bonding with G q residues E242H5.22, Y243H5.23, Q237H5.17, and N244H5.24. As was also seen in the other activated structures, in the (R)-69/5-HT2AR/miniGq/i complex residues A3216.33, L2615.65, I1773.54, L3256.37, and V3246.36 of 5-HT2AR form a hydrophobic core with L236H5.16, L240H5.20, and L245H5.25 of G q. In the complex with (R)-69, as in the earlier activated structures, receptor stabilization by G protein binding includes the rearrangement of ICL2 to a well-structured -helix (Extended Data Fig. 4A).

In the (R)-69 complex, the "toggle switch" residue W3366.48 is in an "upward" conformation that is closer to the inactive LSD bound configuration (PDB: 6WGT16) versus the "downward" configuration observed in the 25CN-NBOH-bound structure (due to the location of the 25CN-NBOH phenol moiety). Nonetheless, W3366.48 is found in the same position in both active structures (Extended Data Fig. 4B) due to the opening of TM6 upon G protein binding with an identical subsequent conformation of the side chain of F3326.44 in the PIF (P5.50-I3.40-F6.44) motif. The PIF motif is known to undergo conformational changes upon receptor activation20. Notably, (R)-69 extends towards TM5 compared to the inactive LSD-bound structure. As also observed for the 25CN-NBOH-bound structure, the (R)-69-bound structure displays an orthosteric binding pocket that is open to the extracellular side of the receptor (Extended Data Fig. 4C, top), compared to a more closed state in the LSD-bound structure16. Interestingly, even though (R)-69 lacks a substituent binding towards the intracellular side of the pocket, a deeper extension of the pocket appears to open between TM3 and TM6 (Extended Data Fig. 4C, bottom). Compared to newly-determined structures of the classic agonists serotonin and psilocin38, which bind relatively high in the orthosteric site of the 5HT2AR, towards its cytoplasmic face, (R)-69 binds about two-rings deeper in the site, more closely engaging recognition residues such as Phe339, Phe340, and Ser242.

Behavioral pharmacology. The potency and selectivity of (R)-69 and (R)-70 prompted us to investigate their biological activities, as drugs that target the 5-HT2AR as antagonists can be used to treat psychosis and other psychiatric indications39, while agonists are reported to exert hallucinogenic, anxiolytic, anti-depressive, and anti-drug abuse actions16,40. There is much interest in finding agonists that retain the anti-depressive effects without the hallucinogenic effects of classic agonists like LSD and psilocin. Encouragingly, both (R)-69 and (R)-70 had substantial brain permeability in mouse PK studies, with injections (i.p.) at 10 mg/Kg leading to gross brain Cmax values of approximately 12 and 35 M, plasma:brain ratios of 1.09 and 0.11, and brain half-lives of 111 and 28.2 min, respectively for (R)-69 and (R)-70 (Ext. Data Figure 5); exposures of the compounds dosed at 1 mg/Kg remained substantial (Ext. Data Figure 5). These favorable CNS exposures prompted us to conduct mouse behavioral studies for head twitch responses (HTRs), classic harbingers of 5-HT2AR engagement41,42. Different doses of both (R)-69 and (R)-70 induced very low levels of HTRs and, with the vehicle control, these values were significantly lower than those for the psychedelic LSD (Figure 5A). Moreover, both (R)-69 and (R)-70 significantly blocked LSD-induced HTRs. We note that the level of inhibition of LSD-induced HTR by (R)-69 and (R)-70 is consistent with what one would expect for a competitive effect at the doses used and given the substantially greater potency of LSD. Since activation of the 5-HT-2AR can lead to hallucinations43, the partial blockade of LSD-induced head twitches with (R)-69 and (R)-70 further demonstrates these compounds are not psychedelics. In an additional test for hallucinogenic actions, different doses of (R)-69 and (R)-70 were found to exert no effects on PPI relative to LSD (Figure 5B; Ext. Data Figure 6A-B Besides finding the hallucinogenic potentials of (R)-69 and (R)-70 were negligible, we tested whether they would acutely stimulate or inhibit locomotion in the open field. Responses to both compounds were not distinguished from the vehicle control (Ext. Data Figure 7A-B). Moreover, both compounds blocked LSD-stimulated hyperlocomotion--further demonstrating they do not possess motor-stimulating activities. In addition, behavioral sensitization and conditioned place preference were not evident with the compounds relative to cocaine (Ext. Data Figure 7C-D). Hence, (R)-69 and (R)-70 do not possess locomotor-stimulating or reinforcing potentials.

Psilocybin and LSD are reported to possess anxiolytic and anti-depressive actions in cancer patients44-47. Accordingly, we tested the effects of (R)-69 and/or (R)-70 in mouse genetic and learned helplessness (LH) models of depressive-like behaviors42. For some of these experiments, we used vesicular monoamine transporter 2 heterozygous mice (VMAT2 HET), which present with motor-retardation in the open field, anhedonia-like behavior to 1 and 1.5% sucrose solutions, enhanced learned helplessness, and augmented stress-induced serum corticosterone levels compared to wild-type (WT) controls. Similarly, in these mice immobility times are increased in the forced swim and tail suspension tests, but are normalized with imipramine, fluoxetine (FLX), reboxetine, and bupropion. Responses to (R)-69 and (R)-70 and several other drugs were examined 30 min and 24 hours post-administration in the VMAT2 HET mice (hashed bars the right of each paired column in Figures 5C and 5D), and compared to WT mice (solid bars on the left of each paired column in Figures 5C and 5D). Examining the first paired columns (Figure 5C and 5D), WT mice treated with vehicle had much lower immobility times than the VMAT2 HET mice both acutely and after 24 h, consistent with the depressive-like phenotype of the mutant mice (significant values between the pair are shown above the columns in all comparisons). In the columns to the right in both panels, the enhanced immobility of the VMAT2 HET animals was normalized by acute administration of FLX, 1 mg/Kg (R)-69, or 0.5 or 1 mg/Kg (R)-70, and it was still at WT vehicle levels 24 h post-administration for both doses of (R)-69 and (R)-70. Thus, in this mouse genetic model both (R)-69 and (R)-70 display anti-depressant-like actions lasting at least over 24 h.

In an effort to determine whether the anti-depressant-like activities of (R)-69 and (R)-70 were mediated through the 5-HT2AR or 5-HT2CR, we administered the antagonists MDL 100907 (MDL) and SB 242084 (SB), respectively. Unfortunately, we found that relative to the vehicle control, both antagonists decreased immobility in the VMAT2 HET mice on their own, confounding interpretation of this experiment (Ext. Data Fig. 6C-D).

To further investigate anti-depressant actions of (R)-70, C57BL/6J mice were tested in a learned helplessness assay (Figure 6A; these experiments were not conducted with (R)-69 owing to reagent limitations). Mice were assigned to foot-shock (FS) and non-FS (NFS) conditions and were given 16 days of training. Subsequently, animals received a single administration (i.p.) of vehicle, 1 mg/Kg (R)-70, 1 mg/Kg psilocin, or 10 mg/Kg ketamine and sucrose preference responses, immobility times, and escape behaviors were examined over time, with anxiety-like behaviors evaluated 13 days post-injection. Prior to drug administration during the pairing of sucrose and water solutions (S-W pairing), mice in the FS condition had a reduced preference for sucrose compared to NFS animals (Figure 6B). Hence, the FS mice exhibited learned helplessness. Following treatment (days 0-20), no significant effects were noted within days among the NFS mice. Crucially, sucrose preference in FS mice was diminished in the vehicle controls versus the (R)-70 and psilocin groups where effects were immediate (acute on day 0) and persisted over 3 days post-injection. Thus, (R)-70 and psilocin

substantially increased preference for sucrose among the FS mice. The corresponding effects of ketamine were not apparent until day 1 but were maintained also through day 3. By day 8 the levels of sucrose preference in all groups were not statistically different. The reduced sucrose preference in FS animals was not due to decreased fluid intake because they drank larger total volumes of the sucrose solution and water than NFS animals prior to treatment, as well as through day 3 post-injection; after day 8 levels of intake were similar between mice in the NFS and FS conditions (Ext. Data Figure 6E).

Relative to sucrose preference, responses to the treatments between and within the FS and NFS conditions were more robust in the tail suspension test. Here, immobility times in the NFS-treated mice were comparable across the 18 days of testing (Figure 6C). By contrast, under the FS condition immobility times were high in the vehicle control relative to the (R)-70 group and this effect persisted through day 14. Compared to the FS vehicle control, psilocin and ketamine were efficacious on days 1 and 4, with the effects of psilocin lasting through day 9 post-injection. Hence, (R)-70 appears to have anti-depressant-like activities not only in the sucrose preference test, but also in the tail suspension test which persisted over days following a single injection.< br>Besides depressive-like responses, anxiety-like behavior was examined. In the elevated zero maze, mice in the FS condition spent less time in the open areas than the NFS mice (Ext. Data Figure 8A). Within the FS condition, vehicle-treated mice spent less time in the open areas than the animals given (R)-70, psilocin, or ketamine. In addition, in the FS mice the latency to enter the open areas was increased, while motor activities in the maze were reduced (Ext. Data Figure 8B-C). Together, these findings suggest the FS mice show anxiety-like behaviors and this is especially apparent in the vehicle-treated mice assigned to the FS condition.

A key aspect of learned helplessness is the animals' performance in escape testing42. This behavior was examined as a function of the numbers of escapes and the latency to escape just prior to treatment (day -1) (Ext, Data Fig. 9A-B). Compared to NFS mice, both indices of escapes were severely affected in the FS mice where they persisted throughout the experiment (i.e., through day 19) and no treatment effects were noted within either the NFS or FS conditions. Together, these results reveal that none of the treatments at the assigned doses could overcome the decrements in escape performance in the FS condition. Moreover, this decrement in performance suggests the FS mice may be presenting not only with depressive- and anxiety-like behaviors, but also with posttraumatic stress disorder-like responses. To determine whether the mice in the NFS or FS conditions or under different treatments were differentially sensitive to foot-shock, all mice were tested for their reactivity to this noxious stimulus (Ext. Data Fig. 9C). Responses of the animals in the FS and NFS conditions were similar to the 0 to 0.3 mAmp stimuli, with responses to the 0.1 to 0.3 mAmp foot-shock being higher than those in the absence of stimulus (i.e., 0 mAmp). No treatment effects were found. Thus, the impairments in escape performance in the FS mice cannot be attributed to differential sensitivities to foot-shock.

Discussion

Here we describe the structure-based screen of a bespoke, ultra-large virtual library of molecules to find functionally-selective agonists with interesting in vitro and in vivo activities. Three observations merit particular emphasis. First, a virtual library of 75 million tetrahydropyridines furnished structures underrepresented in a general-purpose make-on-demand library, with >99% of the molecules in the THP library having no equivalent in the general-purpose library, and 96% representing different scaffolds. Docking this library prioritized molecules active against 5-HT2 receptor subtypes, ultimately leading to potent 5-HT2AR agonists with unusual kinetics for G protein signaling versus arrestin recruitment. Second, the cryo-EM structure of the 5-HT2AR/(R)-69 complex confirms the docking prediction and templates future optimization of this new scaffold. Third, the novelty of (R)-69 and (R)-70 was mirrored in the new biology they conferred, leading to agonists without psychedelic drug-like and locomotor-stimulating actions, typical of classical 5-HT2AR receptor agonists like LSD and psilocin,48 but with anxiolytic-like and strong anti-depressant-like effects in mouse models.

Despite the rapid expansion of make-on-demand libraries, important chemotypes are inevitably under-represented. The tetrahydropyridines explored here exemplify both a chemotype meriting deeper exploration than a general library can afford, and the sort of functionally congested molecule that convergent syntheses can access with great diversity (Figure 1B). We suspect that other scaffolds and synthetic routes may have similar advantages, and we have created a "chemistry commons" for their enumeration and potential exploration via virtual screening (http://commons21.docking.org).

Docking the 75 million lead-like THP library revealed novel ligands, topologically unrelated to those previously known for 5-HT receptors. Four of the initial seventeen THPs synthesized were active against at least one of the 5-HT2R subtypes, a success rate high enough to justify the synthetic effort (Figure 2). Crucially, we were able to leverage SAR from all four hits in a structure-based optimization campaign that led to the potent, selective 5-HT2AR strong partial agonists (R)-69 and (R)-70. Whereas one can qualitatively recognize a serotonergic pharmacophore within these aza-indole tetrahydropyridines—an indole-like ring attached to an ethylamine (here hidden in a ring)—quantitatively, by ECFP4 fingerprints, the new molecules differ from the 15,000 annotated serotonin receptor ligands in ChEMBL, never coming closer than Tanimoto coefficients of 0.25 (SI Figure 5). Inspected by eye, which can sometimes see patterns that fingerprints miss, little similarity emerges to 250 <1 M 5HT2a agonists. Nor do the new agonists resemble widely-studied 5HT2AR agonists like mescaline, LSD, the NBOH family of agonists, lisuride, or psilocin.

From the docking, molecular dynamics (MD), and ultimately free energy perturbation (FEP), we predicted a structure of the 5-HT2AR/(S)-69 complex that was consistent with the molecule's SAR. We note that neither the docking, nor even the subsequent MD, could confidently predict the precise structure of the complex--something complicated by the relatively small size of the 41 nM (R)-69. It was only when we insisted that the complex be consistent with differential affinities among the agonists as probed in the FEP calculations that we accepted a final prediction. Though this predicted pose retained some errors, it closely corresponded to the structure of the 5-HT2AR/(R)-69 complex that was subsequently determined experimentally. This experimental (R)-69/5-HT2AR active-state structure can template the design and further optimization of analogs in this series, potentially improving its promising behavioral pharmacology.

Tetrahydropyridines like (R)-69 are not only strong partial agonists, but unlike psilocybin and LSD, which have substantial polypharmacology across 5-HT receptors31, (R)-69 and (R)-70 also show substantial selectivity for 5-HT2AR, consistent with the new scaffold they represent. Their small size and high ligand efficiency (0.64 kcal/HAC) likely contribute to their high brain permeability when dosed at both 1 and 10 mg/Kg (i.p.) (Extended Data Fig. 5) and, in turn, their efficacy in behavioral studies. Intriguingly, despite their high potencies and efficacies as agonists at 5-HT2ARs, the best compounds were devoid of psychedelic and locomotor-stimulating activities, but they still retained strong anti-depressant-like actions in mouse genetic and stress models, that were equi-efficacious to classic anti-depressants like fluoxetine at as little as 1/40th the dose. This behavior may reflect the distinct kinetics of activation of G protein and Arr recruitment of the new agonists. Our recent findings with LSD33 showed that its psychedelic activities were attenuated in Arr2 knock-out mice, consistent with earlier observations that LSD is βArr-biased21. Thus, our results are consistent with the notion that the differential βArr versus Gq kinetics of (R)-69 and (R)-70 versus those of 5-HT and psilocin are important due to the lack

of psychedelic drug-like actions of these compounds in mice. These distinctions may influence the differential behavioral effects of the compounds, for instance with the effects of (R)-70 becoming apparent acutely and lasting for 14 days in the tail-suspension experiments, while those for psilocin only appear after 24 h and do not last as long. Meanwhile, the NMDA-receptor agonist ketamine also acting as an anti-depressant, shows greater behavioral differences in onset and duration of action in several behavioral assays compared to the two 5-HT2A-R agonists.

Certain caveats merit discussion. Synthetically, the rapid synthesis of highly functionalized, readily diversified scaffolds depends upon facile, convergent, and functional-group-compatible syntheses, limiting the scaffolds suitable for specialized virtual libraries. While the initial docking hit rate for 5-HT2R subtypes was high, at 24%, the hit rate for 5-HT2AR in particular was lower. While the 5-HT2AR/(S)-69 complex was predicted with high-fidelity to the subsequent cryo-EM structure (Figure 4), this demanded extensive MD and FEP simulations;34,49 where docking alone and even pose stability by MD alone50 were insufficient. Rather it was the combination of stable MD geometries50 with FEP based on those geometries that led to the correct prediction. The unusual phenotype of the new agonists—conferring anti-depressant-like activity without apparent hallucinogenic-like activity—may reflect their unusual functional selectivity between G protein and Arr recruitment through the 5HT2A receptor. Admittedly, a role for off-targets, including other 5HT2 subtypes, and even for active metabolites, cannot be excluded. Finally, while the behavioral activity of the new agonists suggests therapeutic potentials, the current molecules demand more exploration and optimization before they can be considered drug candidates.

These caveats should not obscure the central observations of this study. A virtual library of 75 million THPs explored a functionally-congested scaffold underrepresented in general, unbiased make-on-demand libraries. Docking this virtual library prioritized molecules that well-complemented the 5-HT2AR; their optimization led to strong partial agonists with distinct signaling kinetics. As 5-HT2AR agonists, these molecules are potential leads for the development of therapeutics against disorders that have withstood long-term treatment, including depression, anxiety, and posttraumatic stress disorder. More generally, multiple synthetic strategies51 and scaffolds may furnish specialized virtual libraries representing chemotypes unavailable among general make-on-demand libraries. Such focused libraries may illuminate receptors and pharmacologies that have thus far been inaccessible to the community.

Online content

Any methods, additional references, Nature Research reporting summaries, source data, extended data, supplementary information, acknowledgements, peer review information; details of author contributions and competing interests; and statements of data and code availability are available at https://doi.org/10.1038/s41586-022-00000-0

1. Gloriam, D. E. Bigger is better in virtual drug screens. Nature 566, 193-194, doi:10.1038/d41586-019-00145-6 (2019).
2. Lyu, J. et al. Ultra-large library docking for discovering new chemotypes. Nature 566, 224-229, doi:10.1038/s41586-019-0917-9 (2019).
3. Gorgulla, C. et al. An open-source drug discovery platform enables ultra-large virtual screens. Nature 580, 663-668, doi:10.1038/s41586-020-2117-z (2020).
4. Stein, R. M. et al. Virtual discovery of melatonin receptor ligands to modulate circadian rhythms. Nature 579, 609-614, doi:10.1038/s41586-020-2027-0 (2020).
5. Lovering, F., Bikker, J. & Humblet, C. Escape from Flatland: Increasing Saturation as an Approach to Improving Clinical Success. Journal of Medicinal Chemistry 52, 6752-6756, doi:10.1021/jm901241e (2009).
6. The structure, bioactivity, literature, and clinical trials of LSD, ergotamine, vinblastine, vincristine, and dehydroemetine can be obtained by searching the compound name in PubChem.
7. Duttwyler, S., Lu, C., Rheingold, A. L., Bergman, R. G. & Ellman, J. A. Highly Diastereoselective Synthesis of Tetrahydropyridines by a C–H Activation–Cyclization–Reduction Cascade. Journal of the American Chemical Society 134, 4064-4067, doi:10.1021/ja2119833 (2012).
8. Duttwyler, S. et al. Proton Donor Acidity Controls Selectivity in Nonaromatic Nitrogen Heterocycle Synthesis. Science 339, 678, doi:10.1126/science.1230704 (2013).
9. Ischay, M. A., Takase, M. K., Bergman, R. G. & Ellman, J. A. Unstabilized Azomethine Ylides for the Stereoselective Synthesis of Substituted Piperidines, Tropanes, and Azabicyclo[3.1.0] Systems. Journal of the American Chemical Society 135, 2478-2481, doi:10.1021/ja312311k (2013).
10. Boström, J., Brown, D. G., Young, R. J. & Keserü, G. M. Expanding the medicinal chemistry synthetic toolbox. Nature Reviews Drug Discovery 17, 709-727, doi:10.1038/nrd.2018.116 (2018).
11. Sterling, T. & Irwin, J. J. ZINC 15--Ligand Discovery for Everyone. J Chem Inf Model 55, 2324-2337, doi:10.1021/acs.jcim.5b00559 (2015).
12. Oprea, T. I., Davis, A. M., Teague, S. J. & Leeson, P. D. Is there a difference between leads and drugs? A historical perspective. J Chem Inf Comput Sci 41, 1308-1315, doi:10.1021/ci010366a (2001).
13. Berger, M., Gray, J. A. & Roth, B. L. The expanded biology of serotonin. (2009).
14. McCorvy, J. D. & Roth, B. L. Structure and function of serotonin G protein-coupled receptors. (2015).
15. Meltzer, H. Y. & Roth, B. L. Lorcaserin and pimavanserin: emerging selectivity of serotonin receptor subtype-targeted drugs. (2013).
16. Kim, K. et al. Structure of a Hallucinogen-Activated Gq-Coupled 5-HT_{2A} Serotonin Receptor. Cell 182, 1574-1588.e1519, doi:10.1016/j.cell.2020.08.024 (2020).
17. Carhart-Harris, R. et al. Trial of Psilocybin versus Escitalopram for Depression. (2021).
18. Roth, B. L. Drugs and valvular heart disease. (2007).
19. Rothman, R. B. et al. Evidence for possible involvement of 5-HT(2B) receptors in the cardiac valvulopathy associated with fenfluramine and other serotonergic medications. (2000).
20. Wacker, D. et al. Structural features for functional selectivity at serotonin receptors. Science 340, 615-619, doi:10.1126/science.1232808 (2013).
21. Wacker, D. et al. Crystal Structure of an LSD-Bound Human Serotonin Receptor. Cell 168, 377-389 e312, doi:10.1016/j.cell.2016.12.033 (2017).
22. Andrade, R. et al. Vol. 2019(4) (IUPHAR/BPS Guide to Pharmacology, 2019).
23. Mysinger, M. M., Carchia, M., Irwin, J. J. & Shoichet, B. K. Directory of useful decoys, enhanced (DUD-E): better ligands and decoys for better benchmarking. J Med Chem 55, 6582-6594, doi:10.1021/jm300687e (2012).
24. Huang, X. P. et al. Allosteric ligands for the pharmacologically dark receptors GPR68 and GPR65. Nature 527, 477-483, doi:10.1038/nature15699 (2015).
25. Lansu, K. et al. In silico design of novel probes for the atypical opioid receptor MRGPRX2. Nat Chem Biol 13, 529-536, doi:10.1038/nchembio.2334 (2017).
26. Irwin, J. J. & Shoichet, B. K. Docking Screens for Novel Ligands Conferring New Biology. J Med Chem 59, 4103-4120, doi:10.1021/acs.jmedchem.5b02008 (2016).
27. Bento, A. P. et al. The ChEMBL bioactivity database: an update. Nucleic Acids Res 42, D1083-1090, doi:10.1093/nar/gkt1031 (2014).
28. Yempala, T. et al. Dibenzofuranylethylamines as 5-HT2A/2C Receptor Agonists. ACS Omega 5, 2260-2266, doi:10.1021/acsomega.9b03430 (2020).
29. Xu, P. et al. Structural insights into the lipid and ligand regulation of serotonin receptors. Nature 592, 469-473, doi:10.1038/s41586-021-03376-8 (2021).
30. Lassalas, P. et al. Evaluation of Oxetan-3-ol, Thietan-3-ol, and Derivatives Thereof as Bioisosteres of the Carboxylic Acid Functional Group. ACS Medicinal Chemistry Letters 8, 864-868, doi:10.1021/acsmedchemlett.7b00212 (2017).
31. Kroeze, W. K. et al. PRESTO-Tango as an open-source resource for interrogation of the druggable human GPCRome. Nature Structural & Molecular Biology 22, 362-369, doi:10.1038/nsmb.3014 (2015).
32. Ray, T. S. Psychedelics and the Human Receptorome. PLOS ONE 5, e9019, doi:10.1371/journal.pone.0009019 (2010).
33. Rodriguiz, R. M. et al. LSD-stimulated behaviors in mice require beta-arrestin 2 but not beta-arrestin 1. Sci Rep 11, 17690, doi:10.1038/s41598-021-96736-3 (2021).
34. Abel, R., Wang, L., Harder, E. D., Berne, B. J. & Friesner, R. A. Advancing Drug Discovery through Enhanced Free Energy Calculations. Accounts of Chemical Research 50, 1625–1632, doi:https://doi.org/10.1021/acs.accounts.7b00083 (2017).
35. Ballesteros, J. A. & Weinstein, H. in Methods in Neurosciences Vol. 25 (ed Stuart C. Sealfon) 366-428 (Academic Press, 1995).
36. Maeda, S. et al. Development of an antibody fragment that stabilizes GPCR/G-protein complexes. Nature Communications 9, 3712, doi:10.1038/s41467-018-06002-w (2018).
37. Robertson, M. J., van Zundert, G. C. P., Borrelli, K. & Skiniotis, G. GemSpot: A Pipeline for Robust Modeling of Ligands into Cryo-EM Maps. Structure 28, 707-716.e703, doi:https://doi.org/10.1016/j.str.2020.04.018 (2020).
38. Cao, D. et al. Structure-based discovery of nonhallucinogenic psychedelic analogs. Science 375, 403-411, doi:10.1126/science.abl8615 (2022).
39. Meltzer, H. Y. The role of serotonin in antipsychotic drug action. (1999).
40. Nutt, D., Erritzoe, D. & Carhart-Harris, R. Psychedelic Psychiatrys Brave New World. (2020).
41. Corne, S. J. & Pickering, R. W. A possible correlation between drug-induced hallucinations in man and a behavioural response in mice. (1967).
42. Woolley, D. W. Production of Abnormal (Psychotic?) Behavior in Mice with Lysergic Acid Diethylamide, and Its Partial Prevention with Cholinergic Drugs and Serotonin. Proc Natl Acad Sci U S A 41, 338-344, doi:10.1073/pnas.41.6.338 (1955).
43. Roth, B. L., Willins, D. L., Kristiansen, K. & Kroeze, W. K. Activation is Hallucinogenic and Antagonism is Therapeutic: Role of 5-HT2A Receptors in Atypical Antipsychotic Drug Actions. The Neuroscientist 5, 254-262, doi:10.1177/107385849900500414 (1999).
44. Gasser, P., Kirchner, K. & Passie, T. LSD-assisted psychotherapy for anxiety associated with a life-threatening disease: a qualitative study of acute and sustained subjective effects. J Psychopharmacol 29, 57-68, doi:10.1177/0269881114555249 (2015).
45. Goldberg, S. B., Pace, B. T., Nicholas, C. R., Raison, C. L. & Hutson, P. R. The experimental effects of psilocybin on symptoms of anxiety and depression: A meta-analysis. Psychiatry Res 284, 112749, doi:10.1016/j.psychres.2020.112749 (2020).

46. Grob, C. S. et al. Pilot study of psilocybin treatment for anxiety in patients with advanced-stage cancer. Arch Gen Psychiatry 68, 71-78, doi:10.1001/archgenpsychiatry.2010.116 (2011).
47. Ross, S. et al. Rapid and sustained symptom reduction following psilocybin treatment for anxiety and depression in patients with life-threatening cancer: a randomized controlled trial. J Psychopharmacol 30, 1165-1180, doi:10.1177/0269881116675512 (2016).
48. Shao, L. X. et al. Psilocybin induces rapid and persistent growth of dendritic spines in frontal cortex in vivo. Neuron, doi:10.1016/j.neuron.2021.06.008 (2021).
49. Jorgensen, W. L. Efficient drug lead discovery and optimization. Acc Chem Res 42, 724-733, doi:10.1021/ar800236t (2009).
50. Cutrona, K. J., Newton, A. S., Krimmer, S. G., Tirado-Rives, J. & Jorgensen, W. L. Metadynamics as a Postprocessing Method for Virtual Screening with Application to the Pseudokinase Domain of JAK2. J Chem Inf Model 60, 4403-4415, doi:10.1021/acs.jcim.0c00276 (2020).
51. Saper, N. I. et al. Nickel-catalysed anti-Markovnikov hydroarylation of unactivated alkenes with unactivated arenes facilitated by non-covalent interactions. Nat Chem 12, 276-283, doi:10.1038/s41557-019-0409-4 (2020).
52. Pei, J. & Grishin, N. V. PROMALS3D: multiple protein sequence alignment enhanced with evolutionary and three-dimensional structural information. Methods Mol Biol 1079, 263-271, doi:10.1007/978-1-62703-646-7_17 (2014).
53. Liu, W. et al. Serial femtosecond crystallography of G protein-coupled receptors. Science 342, 1521-1524, doi:10.1126/science.1244142 (2013).
54. Webb, B. & Sali, A. Comparative Protein Structure Modeling Using MODELLER. Current protocols in bioinformatics / editoral board, Andreas D. Baxevanis ... [et al.] 47, 5 6 1-5 6 32, doi:10.1002/0471250953.bi0506s47 (2014).
55. Coleman, R. G., Carchia, M., Sterling, T., Irwin, J. J. & Shoichet, B. K. Ligand pose and orientational sampling in molecular docking. PLoS One 8, e75992,doi:10.1371/journal.pone.0075992 (2013).
56. Southan, C. et al. The IUPHAR/BPS Guide to PHARMACOLOGY in 2016: towards curated quantitative interactions between 1300 protein targets and 6000 ligands. Nucleic Acids Res 44, D1054-1068, doi:10.1093/nar/gkv1037 (2016).
57. Case, D. A. et al. AMBER 2015. (2015).
58. Mysinger, M. M. & Shoichet, B. K. Rapid context-dependent ligand desolvation in molecular docking. J Chem Inf Model 50, 1561-1573, doi:10.1021/ci100214a (2010).
59. Wei, B. Q., Baase, W. A., Weaver, L. H., Matthews, B. W. & Shoichet, B. K. A model binding site for testing scoring functions in molecular docking. J Mol Biol 322, 339-355, doi:10.1016/s0022-2836(02)00777-5 (2002).
60. Word, J. M., Lovell, S. C., Richardson, J. S. & Richardson, D. C. Asparagine and glutamine: using hydrogen atom contacts in the choice of side-chain amide orientation1. Journal of Molecular Biology 285, 1735-1747, doi:http://dx.doi.org/10.1006/jmbi.1998.2401 (1999).
61. Gallagher, K. & Sharp, K. Electrostatic contributions to heat capacity changes of DNA-ligand binding. Biophys J 75, 769-776, doi:10.1016/S0006-3495(98)77566-6 (1998).
62. Sharp, K. A. Polyelectrolyte electrostatics: Salt dependence, entropic, and enthalpic contributions to free energy in the nonlinear Poisson–Boltzmann model. Biopolymers 36, 227-243, doi:10.1002/bip.360360210 (1995).
63. Pettersen, E. F. et al. UCSF Chimera—A visualization system for exploratory research and analysis. Journal of Computational Chemistry 25, 1605-1612, doi:https://doi.org/10.1002/jcc.20084 (2004).
64. Olsson, M. H. M., Søndergaard, C. R., Rostkowski, M. & Jensen, J. H. PROPKA3: Consistent Treatment of Internal and Surface Residues in Empirical PKa Predictions. Journal of Chemical Theory and Computation 7, 525–537 (2011).
65. Wang, L. et al. Accurate and Reliable Prediction of Relative Ligand Binding Potency in Prospective Drug Discovery by Way of a Modern Free-Energy Calculation Protocol and Force Field. J Am Chem Soc 137, 2695–2703 (2015).
66. Olsen, R. H. J. et al. TRUPATH, an open-source biosensor platform for interrogating the GPCR transducerome. Nature Chemical Biology 16, 841-849, doi:10.1038/s41589-020-0535-8 (2020).
67. Zhang, Y., Yang, Z., Gao, X. & Wu, G. The role of 5-hydroxytryptamine1A and 5-hydroxytryptamine1B receptors in modulating spinal nociceptive transmission in normal and carrageenan-injected rats. Pain 92, 201-211, doi:10.1016/s0304-3959(01)00259-7 (2001).
68. Mastronarde, D. N. Automated electron microscope tomography using robust prediction of specimen movements. J Struct Biol 152, 36-51 (2005).
69. Zivanov, J. et al. New tools for automated high-resolution cryo-EM structure determination in RELION-3. eLife 7, e42166, doi:10.7554/eLife.42166 (2018).
70. Zheng, S. Q. et al. MotionCor2: anisotropic correction of beam-induced motion for improved cryo-electron microscopy. Nature Methods 14, 331-332, doi:10.1038/nmeth.4193 (2017).
71. Emsley, P., Lohkamp, B., Scott, W. G. & Cowtan, K. Features and development of Coot. Acta Crystallographica Section D 66, 486-501, doi:doi:10.1107/S0907444910007493 (2010).
72. Liebschner, D. et al. Macromolecular structure determination using X-rays, neutrons and electrons: recent developments in Phenix. Acta Crystallographica Section D 75, 861-877, doi:doi:10.1107/S2059798319011471 (2019).
73. Williams, C. J. et al. MolProbity: More and better reference data for improved all-atom structure validation. Protein Science 27, 293-315, doi:https://doi.org/10.1002/pro.3330 (2018).
74. Pettersen, E. F. et al. UCSF ChimeraX: Structure visualization for researchers, educators, and developers. Protein Science 30, 70-82, doi:https://doi.org/10.1002/pro.3943 (2021).
75. Fukui, M. et al. Vmat2 heterozygous mutant mice display a depressive-like phenotype. J Neurosci 27, 10520-10529, doi:10.1523/JNEUROSCI.4388-06.2007 (2007).
76. Berezniuk, I. et al. ProSAAS-derived peptides are regulated by cocaine and are required for sensitization to the locomotor effects of cocaine. J Neurochem 143, 268-281, doi:10.1111/jnc.14209 (2017).
77. Pogorelov, V. M. et al. 5-HT2C Agonists Modulate Schizophrenia-Like Behaviors in Mice. Neuropsychopharmacology 42, 2163-2177, doi:10.1038/npp.2017.52 (2017).
78. Wetsel, W. C. et al. Disruption of the expression of the proprotein convertase PC7 reduces BDNF production and affects learning and memory in mice. Proc Natl Acad Sci U S A 110, 17362-17367, doi:10.1073/pnas.1314698110 (2013).